Available online at www.sciencedirect.com

ScienceDirect

Energy Procedia 70 (2015) 285 – 292

Energy Procedia

International Conference on Solar Heating and Cooling for Buildings and Industry, SHC 2014

Numerical investigation of flow and heat transfer performance of solar water heater with elliptical collector tube

Kaichun Li[a], Tong Li[b], Hanzhong Tao[a,b,] *,Yuanxue Pan[a],Jingshan Zhang[a]

[a]*Sunrain Group Co.,Ltd,Lianyungang,222243,China*
[b]*College of Energy, Nanjing Tech University, Nanjing 211816, China*

Abstract

The flow and heat transfer performance of solar water heaters for different initial temperatures (273K, 283K, 293K, 303K and 313K) with elliptical collector tubes are evaluated using numerical simulation. The predicted results match fairly well with experimental data. Results indicate that, the temperature distributions of all the tube cross sections are alike, but the velocity profiles of them are much dissimilar. The fluid velocity near the wall decrease with decrease in the ratio of the cross section major and minor axis, which induces the reduction in the circulation rate through the collector tubes, which is not conducive to heat transfer. The mean Nusselt number of solar water heater with b/a=1 (b and a here are respectively major and minor axis of collector tube cross section) are respectively 59% and 19% larger than the solar water heaters withb/a=0.6 and 0.8 for the temperature ranging from 273K to 313K.

Peer-review by the scientific conference committee of SHC 2014 under responsibility of PSE AG

Keywords: Numerical simulation; Solar water heater; Heat transfer;

1. Introduction

Solar water heater is widely used all over the world due to its simplicity, technological feasibility, economical and commercial viability. Extensive and systematic researches have been carried out over the years to evaluate the performance of the solar water heater [1-4]. Jaisankar et al. [5] experimentally investigated the friction factor and heat transfer characteristics of thermosyphon solar water heater with full length Left-Right twist, twist fitted with rod and spacer at the trailing edge, results showed that the solar water heaters with full length twists are better for heat

* Corresponding author. Tel.: +86 13776668774;.
*E-mail address:*taohanzhong@njtech.edu.cn

Peer-review by the scientific conference committee of SHC 2014 under responsibility of PSE AG
doi:10.1016/j.egypro.2015.02.125

transfer and with lower flow resistance than the other two. Morrison et al. [6] developed a numerical model of the heat transfer and flow inside a single-ended evacuated tube to evaluate the characteristics of water-in-glass evacuated tube solar water heater, results showed that, the natural convection flow rate in the tube is high enough to disturb the tank's stratification and that the tank temperature strongly affects the circulation flow rate through the tubes. Budihardjo et al. [7] undertake experimental and numerical investigations to develop a correlation for natural circulation flow rate through single-ended water-in-glass evacuated tubes mounted over a diffuse reflector. The circulation flow rate was correlated in terms of solar input, tank temperature, collector inclination and tube aspect ratio. The sensitivity of the flow rate correlation to the variation in circumferential heat flux distribution was also investigated. Yan et al. [8, 9] numerically and experimentally studied the effect of irradiance, tilt angle and the guide plate on the heat transfer performance, based on the results of the study, they proposed many suggestions for optimization of the solar water heater.

With the popularity of wall hanging solar water heater, there will be security threat because of the large weight of the collector. The potential safety hazard may be reduced if the circular collector tube changed into elliptic pipe, which make the weight of the collector tube lower. In this paper, the flow and heat transfer performance of solar water heaters with elliptical collector tubes are evaluated and compared with the normal one using CFD.

Nomenclature

D	circular tube diameter (m)	h	heat transfer coefficient (W/m^2·K)
a	minor axis of elliptical cross section (m)	A	heat transfer surface area (m^2)
b	major axis of elliptical cross section (m)	T_W	average wall temperature (K)
L	length of collector tube (m)	T_b	average bulk temperature (K)
D_T	inner diameter of tank (m)	Nu	Nusselt number
T	fluid temperature (K)	d	equivalent diameter of collector tube (m)
c_p	specific heat of fluid (J/kg ·K)	g	acceleration of gravity (m/s^2)
k	thermal conductivity (W/m ·K)	p	static pressure (Pa)
Q	heat transfer rate (W)	q_W	average heat input into the tube (W/m^2)
m	mass flow rate (kg/s)	α	tilt angle of the solar water heater (°)
T_{in}	inlet temperature of tank (K)	ρ	density (kg/m^3)
T_{out}	outlet temperature of tank (K)	μ	dynamic viscosity (kg/m ·s)

2. Numerical method

2.1. Physical model

The inner tube of the all glass evacuated solar collector tube used in this paper was elliptical tube, and the outer one was circular tube. The general structure of the inner tube cross section of the collector tube was shown in Fig.1. The major axis of the all tubes were 0.047m, the minor axis of the tubes were respectively 0.047m, 0.0376m and 0.0282m. In the other words, the ratios of the minor axis and major axis were respectively 1, 0.8 and 0.6. The length of the collector L was 1.8m, the inner diameter of tank was 0.36m, and the tilt angle of the solar collector was 45°. The thermophysical property of the working fluid, water, was shown in Table 1. The properties between them get from line interpolation.

Table 1 Thermophysical property of water

T (K)	ρ (kg/m3)	c_p (J/kg · K)	k (W/m · K)	μ (kg/m·s)
273	999.9	4212	0.551	0.001788
283	999.7	4191	0.574	0.001306
293	998.2	4183	0.599	0.001004

303	995.7	4174	0.618	0.0008015
313	992.2	4174	0.635	0.0006533
323	988.1	4174	0.648	0.0005494

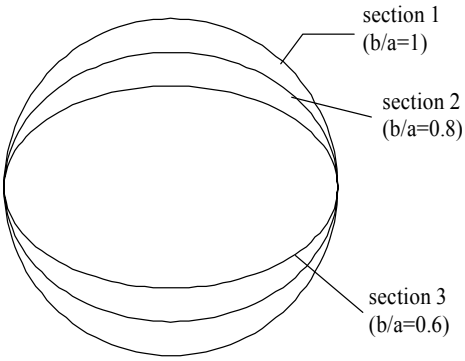

Fig. 1 Cross sections of the collector tubes

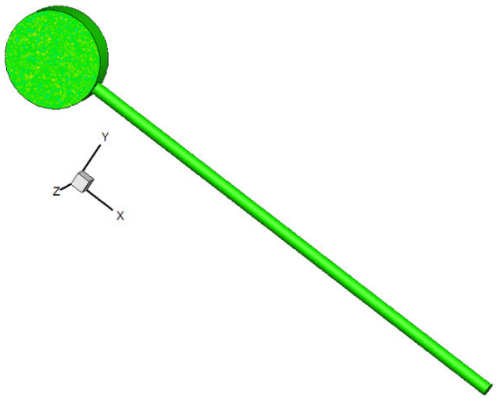

Fig. 2 Computational domain

2.2. Data reduction

The data is reduced in the following procedure. Firstly, the total heat transfer rate can be obtained by

$$Q = mc_p(T_{out} - T_{in}) \tag{1}$$

T_{in} and $T_{out}$are calculated using

$$T = \frac{\sum_{i=1}^{n} T_i \rho_i \left|\vec{u_i} \cdot \vec{A_i}\right|}{\sum_{i=1}^{n} \rho_i \left|\vec{u_i} \cdot \vec{A_i}\right|} \tag{2}$$

where T_i, ρ_i, $\vec{u_i}$, $\vec{A_i}$ are respectively temperature, density, velocity vector and area vector of area element i which on the inlet or outlet of the tank.

The heat transfer coefficient is determined by

$$h = Q / \left[A\left(T_w - T_b\right)\right] \tag{3}$$

$$T_b = \left(T_{in} + T_{out}\right) / 2 \tag{4}$$

The Nu is calculated from

$$Nu = hd / k \tag{5}$$

2.3. Numerical model

Some assumptions are used to simplify the problem: (1) the radiation intensity is almost uniform on the top half of the tube, and the bottom half is thermally insulated, (2) the tank has good heat-retaining performance, the heat loss through the insulation layer is zero, (3) the tank is positioned horizontally and all the walls are hydraulically, (4) there is no heat exchange between the evacuated collector tube and outside surrounding due to its good vacuum quality, (5) the tank is full of water and no air, (6) the flow in the whole computational domain is laminar. The numerical model used in this paper is a single tube connected to tank, the whole computational domain as shown in Fig. 2. For simplicity, the model considered the inner tube and the outer tube was neglected. In addition, the heat transformed from the radiation replaced by the uniform heat input.

2.4. Mesh design

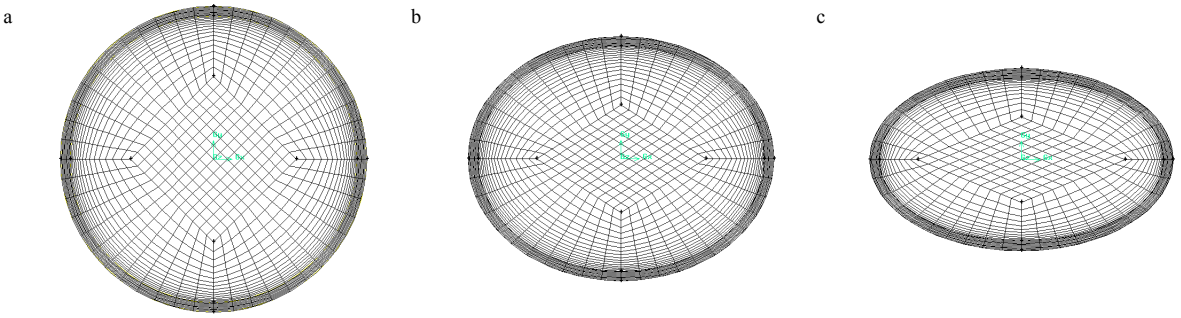

Fig. 3 Meshed geometry of the tube cross sections (a) b/a=1; (b) b/a=0.8; (c) b/a=0.6

Grid generation is a key issue in numerical simulation as it governs the stability, economy and accuracy of the predictions. The meshed geometry of the tube cross sections are shown in Fig. 3. Considering the steeper gradient near the wall, finer mesh was meshed near the wall. A mesh independence test was carried out by comparison of Nu for different mesh sizes. Three grid systems with about 870000, 1510000 and 2690000 nodes are adopted to calculate a baseline case in which b/a=1, T=313K. The Nuseelt numbers of the baseline case are shown in Fig. 4, which demonstrates that the difference between the calculated results of 1510000 and 2690000 nodes is very small. Therefore, the grid system with 1510000 nodes is adopted for the following calculations.

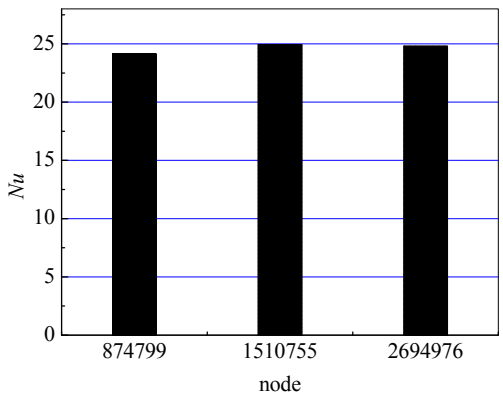

Fig. 4 Mesh independence test

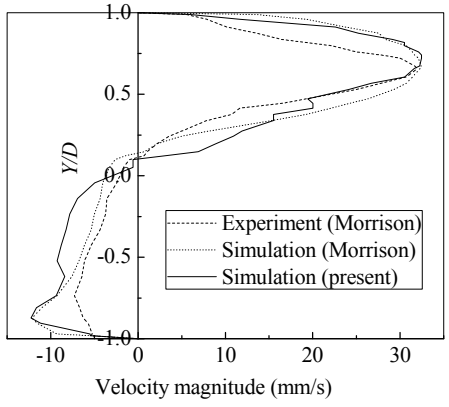

Fig. 5 Comparison of present results and Morrison's results

2.5. Governing equations

The problem under consideration is assumed to be three-dimensional, laminar and steady. Equations of continuity, momentum and energy for the fluid flow are given below in a tensor form,

Continuity equation:

$$\frac{\partial\left(\rho u_i\right)}{\partial x_i}=0 \tag{6}$$

Momentum equation:

$$\frac{\partial\left(\rho u_i u_j\right)}{\partial x_j}=\frac{\partial}{\partial x_j}\left(\mu\frac{\partial u_i}{\partial x_j}\right)-\frac{\partial p}{\partial x_i}+\rho g_i \tag{7}$$

Energy equation:

$$\frac{\partial}{\partial x_i}\left(\rho u_i C_p T-k\frac{\partial T}{\partial x_i}\right)=0 \tag{8}$$

2.6. Boundary conditions and solution scheme

At the computational domain of inlet and outlet, periodical condition is imposed, which indicates that the velocity, pressure and temperature gradient repeat themselves in the domain as follows:

$$u_i\left(\vec{r}\right)=u_i\left(\vec{r}+\vec{L}\right)=u_i\left(\vec{r}+2\vec{r}\right)=\ldots \tag{9}$$

$$\Delta p=p\left(\vec{r}\right)-p\left(\vec{r}+\vec{L}\right)=p\left(\vec{r}+\vec{L}\right)-p\left(\vec{r}+2\vec{L}\right)=\ldots \tag{10}$$

$$\sigma=\frac{T\left(\vec{r}+\vec{L}\right)-T\left(\vec{r}\right)}{L}=\frac{T\left(\vec{r}+2\vec{L}\right)-T\left(\vec{r}+\vec{L}\right)}{L}=\ldots \tag{11}$$

where $\vec{r}$, $\vec{L}$, Δp and σ are respectively position vector, length vector of a period, pressure drop of a period and temperature of a period. The mass flow rate through the inlet and outlet is 0.02kg/s.

No slip condition is applied on all the walls, that is, the velocity magnitude near the wall is zero:

$$u_i=0 \tag{12}$$

Uniform heat flux condition is imposed on the top half of the tube wall:

$$q=q_w \tag{13}$$

where $q_W=750W/m^2$. All the other walls are thermally insulated.

In the present study, the governing equations were solved with the finite volume approach. The second order

upwind scheme was used to discrete momentum and energy equation. A Body Force Weighted interpolation method was imposed for pressure. The coupling between the pressure and velocity field was established using SIMPLE algorithm. The solution convergence is achieved by a criterion for the normalized residuals below 10^{-6} for energy and 10^{-3} for other equations.

To validate the accuracy of the numerical solutions, the predicted results in this paper are compared with the experimental and numerical results of Morrison [6] under similar condition. From Fig. 5 it is clearly seen that the deviation between the results is very limited. Therefore, the present numerical simulations have reasonable accuracy.

3. Results and discussions

3.1. Flow structure

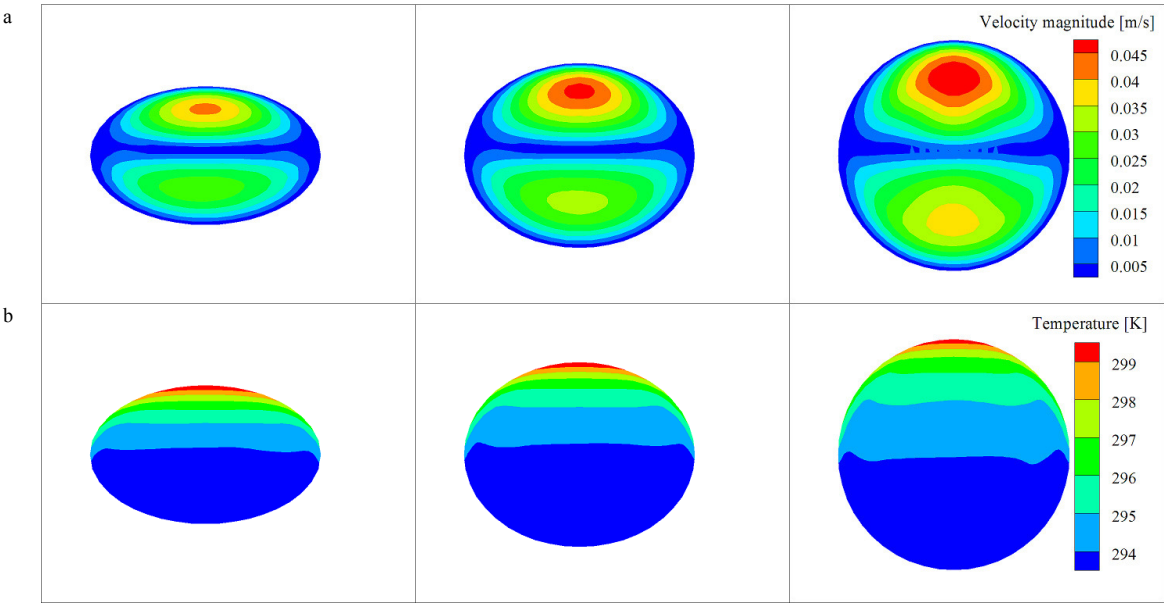

Fig. 6 (a) Velocity counters and (b) temperature counters of the cross sections

Fig.6 shows the velocity and temperature counters of the tube cross sections which $L/3$ away from the tanks (the initial temperature is 293K). It can be seen that, as heated by the top half of the tube wall, the water near the top half of the tube wall flow toward the tank driven by the body force due to the density decrease. At the same time, the water near the bottom half of the tube wall flow downward driven by gravity due to its larger density. For this reason, the velocity of the water near the tube wall is higher than other regions. Furthermore, the velocity of the water near the top half of the tube wall is higher than the water near the bottom half of the tube wall due to its higher temperature. Since the water near the top and bottom half of the tube wall flow in opposite directions, a shear layer is formed between them. And the shear layer has the smallest velocity. It can also be seen that all the cross sections have similar temperature distributions. However, the velocity distributions of the cross sections are different from each other. From Fig. 6 (a) it can be seen that the velocity decrease with the decrease in the ratio of major axis and minor axis of the elliptical cross section, it will induce the reduction of circulation rate which is not conducive to heat transfer.

Fig. 7 depicts the variation of mean velocity magnitudes of eighteen cross sections, namely, $L^{/}/L$ = 0, 0.06, 0.11, 0.17, 0.22 until 0.94, where $L^{/}$ is the distance of the cross section away from the tank. From Fig. 7, it can be seen that the mean velocity magnitude near the tank is smaller than the region range from 0.06L to 0.4L. The explanation for this phenomenon is that, the upward hot water is cooled by the downward cold water and it will lead the hot

water to flow in the opposite direction due to the smaller density, at the same time, the cold water is heated by the hot water, and the cold water will flow upward due to the increment in density, all these can lead to the generation of short current flow. The velocity magnitude in the domain range from 0.06*L* to 0.4*L* is larger because of the higher temperature. The mean velocity magnitude is become smaller from 0.4*L* to the bottom of the tube. This is because the cold water is heated in the process of flowing to the bottom of the tube, and it is carried off by the upward hot flow before reaching the tube bottom. Another feature can be seen from Fig. 7 is that the mean velocity magnitude increase with increment in the ratio of major axis and minor axis of the tube cross section, which indicates excellent agreement with Fig. 6.

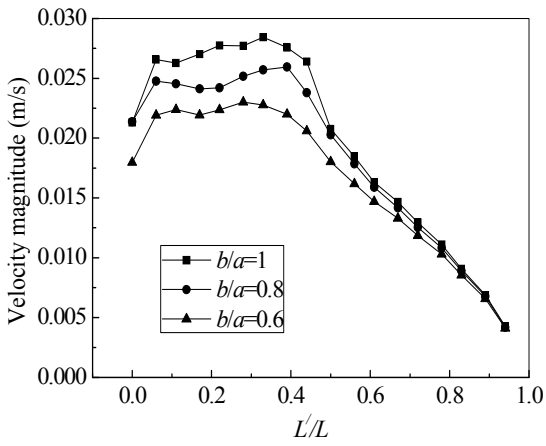

Fig. 7 Variation of mean velocity magnitudes of the cross sections

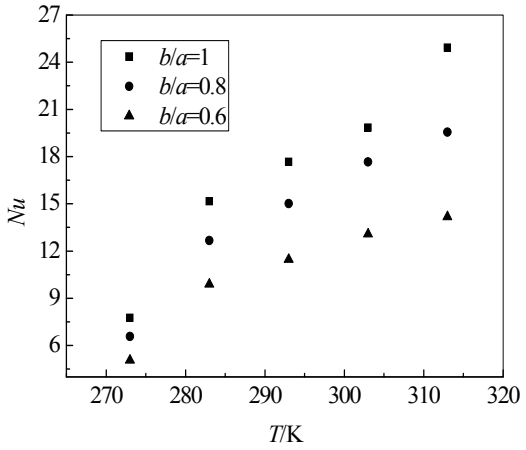

Fig. 8 Variation of Nuseelt number of the solar water heaters

3.2. Heat transfer

Fig. 8 presents the variation in the Nuseelt number of the three solar water heaters at different initial temperatures. It can be seen that the value of Nuseelt number increase with increment in initial temperature. This is because the higher temperature leads to a higher circulation rate, which makes heat transfer better. The Nuseelt numbers of the solar water heaters with *b*/*a*=1, 0.8 and 0.6 are respectively increase by 2.21, 1.98 and 1.80 times for the initial temperature ranging from 273K to 313K. Moreover, it can also be seen that, the larger the value of *b*/*a*, the better heat transfer is, which is agree with Fig. 6 and 7. Over the range investigated, the mean Nuseelt number of the solar water heater with *b*/*a*=1 is respectively 59% and 19% larger than the solar water heaters with *b*/*a*=0.6 and 0.8. Consequently, although the solar water heater with elliptical collector tube is ahead of the normal solar water heater in some ways, but, as to flow and heat transfer performance, the normal solar water heater do better than it.

4. Conclusion

The flow and heat transfer performance of solar water heaters for different initial temperatures (ranging from 273K to 313K) with elliptical collector tubes are evaluated and compared with normal solar water heater using numerical simulation. The predicted results match fairly well with experimental data. Results indicate that, the temperature distributions of all the tube cross sections are similar, but the velocity profiles of them are much dissimilar. The fluid velocity near the wall and decrease with decrease in the ratio of the cross section major and minor axis, which induces the reduction in the circulation rate through the collector tubes, which is not conducive to heat transfer. The value of Nuseelt number increase with increment in initial temperature. The larger the value of *b*/*a*, the better heat transfer is. Over the range investigated, the mean Nusselt number of solar water heater with *b*/*a*=1are

respectively 59% and 19% larger than the solar water heaters withb/a=0.6 and 0.8 for the temperature ranging from 273K to 313K.

References

[1] Morrison GL, Budihardjo I, Behnia M. Water-in-glass evacuated tube solar water heaters. Solar Energy 2004;76:135-140.
[2] Ananth J, Jaisankar S. Experimental studies on heat transfer and friction factor characteristics of thermosyphon solar water heating system fitted with regularly spaced twistd tape with rod and spacer. Energy Conversion and Management 2013;73:207-213.
[3] Tang RS, Gao WF, Yu YM, Chen H. Optimal tilt-angles of all-glass evacuated tube solar collectors. Energy 2009;34:1387-1395.
[4] Yadav A, Bajpai VK. An experimental study on evacuated tube solar collector for heating of air in India. 2011;79:81-86.
[5] Jaisankar S, Radhakrishnan TK, Sheeba KN, Suresh S. Experimental investigation of heat transfer and friction factor characteristics of thermosyphon solar water heater system fitted with spacer at the trailing edge of Left-Right twisted tapes. Energy Conversion and Management 2009;50:2638-2649.
[6] Morrison GL, Budihardjo I, Behnia M. Measurement and simulation of flow rate in a water-in-glass evacuated tube solar water heater. Solar Energy 2005;78:257-267.
[7] Budihardjo I, Morrison GL, Behnia M. Natural circulation flow through water-in-glass evacuated tube solar collectors. Solar Energy 2007;81:1460-1472.
[8] Yan SY, Huang HY, Tian R, Zhang WW, Yu WY. Mechanism analysis for the heat transfer enhancement with all-glass vacuum tube solar water heaters. Journal of Engineering Thermophysics 2012;33:485-488(in Chinese).
[9] Yan SY, Tian R, Yu WY, Li S. Analysis on factors influencing fluid flow in an all-glass vacuum tube solar water heaters. Journal of Engineering Thermophysics 2010;31:641-643(in Chinese).